Two-wave-plate compensator method for single-point retardation measurements

Carole C. Montarou and Thomas K. Gaylord

The two-wave-plate compensator (TWC) technique is introduced for single-point retardation measurements. The TWC method uses a known wave plate together with a wave plate of unknown retardation and produces a linearly polarized output that allows a null of intensity to be detected. The TWC method is compared both theoretically and experimentally with the existing Brace–Köhler and Sénarmont methods. The resolution of the TWC is shown to be 0.02 nm. TWC enables the measurement of a sample retardation with as little as 0.13% error and thus is more accurate than either the Brace–Köhler or the Sénarmont method. © 2004 Optical Society of America

OCIS codes: 230.7370, 260.1440, 260.5430.

1. Introduction

Natural or induced birefringence magnitude and orientation are directly related to the characteristics of optical materials, devices, or living cells. Accurate measurements of the retardation therefore leads to the characterization of the sample's physical properties in a wide range of applications such as in crystallography for the determination of lattice mismatch,[1–3] in biology for the dynamic observation of living cells,[4,5] for the early detection of glaucoma in the human eye,[6] in quality control of transparent materials for the measurement of stress level in glass and plastic,[7,8] in optical communications for the evaluation of residual stress or polarization mode dispersion in micro-electrical mechanical systems,[9,10] in optical fibers,[11–26] and in optical interconnects.[27–30]

Several techniques have been developed to measure retardation magnitude and orientation. Photoelastic measurements involve the use of circular polariscopes, i.e., polarizers and quarter-wave plates, together with intensity measurements to retrieve the retardation magnitude of a sample.[31] The use of quarter-wave plates affects the accuracy of the technique, especially when it is used in white light.[32] Based on photoelasticity, spectral content analysis uses a circular polariscope and a CCD camera in white light to allow full-field retardation measurements.[7,8] These techniques cannot detect low-level birefringence such as that present in optical fibers and waveguides.

Recently, photoelastic modulators have been used to modulate the polarization state of the light traveling through an optical system composed of polarizers and the sample under investigation. It has been shown that the frequency demodulation of the transmitted optical signal leads to accurate measurements of the low-level retardation magnitude and orientation of the sample.[33,34] This technique, however, possesses a low spatial resolution of the order of a millimeter, which renders impossible the profiling of devices such as optical fibers and waveguides.

In biology, polarization microscopy has proven to be very effective in detecting low-level birefringence in living cells.[35,36] The use of compensators allows the detection of low-level birefringence.[35] More recently, a new liquid-crystal-based compensator has been added to a polarization microscope to allow the detection of low-level retardation magnitude and orientation in living cells.[37] The technique relies, however, on the accurate measurement of the light intensity, and the compensator used is not a conventional, commercially available compensator.

Another well-known technique to measure low-level birefringence is based on the Brace–Köhler compensator. The method consists of finding a minimum of intensity by rotating a compensator plate when a sample is observed between crossed polarizers. The technique, however, uses a small-retardation approximation, and an intensity minimum is found rather than complete extinction. This

The authors are with the School of Electrical and Computer Engineering, Georgia Institute of Technology, 777 Atlantic Drive NW, Atlanta, Georgia 30332-0250. T. Gaylord's e-mail address is tgaylord@ece.gatech.edu.

Received 10 February 2004; accepted 11 May 2004.
0003-6935/04/366580-16$15.00/0

adversely affects the accuracy of the measurement. Furthermore, the Brace–Köhler compensator technique assumes that the sample retardation orientation is known.

When using monochromatic light for low-level retardation measurements, there is a need for a method based on finding a null of intensity that is more accurately measurable than an intensity minimum or an absolute light intensity. The method should not make any approximations about the retardation of the sample.

In this research, the two-wave-plate compensator (TWC) is analyzed and compared with the existing Brace–Köhler and Sénarmont techniques for single-point retardation measurements. The first part of this paper deals with a thorough analysis of the Brace–Köhler method. The shortcomings of the method are identified. The second part of this paper deals with a thorough analysis of the TWC technique, which consists of rotating a wave plate in a two-wave-plate system until a linearly polarized output is produced. This allows a null of intensity to be measured by rotating an analyzer perpendicular to the electric field polarization direction. The applicability range, error, resolvability limit, and resolution are also quantified. Detailed experimental procedures are developed to apply the method to single-point retardation measurements. The TWC technique is also compared experimentally to the Brace–Köhler and Sénarmont techniques using samples with small retardations.

2. Brace–Köhler Compensator

The Brace–Köhler compensator retardation-measurement method, also known as the elliptic compensator method, consists of finding a minimum of intensity by rotating a compensator wave plate in order to determine the sample retardation. The two wave plates are placed between crossed polarizers. With the sample at 45° from extinction, the compensator angle producing a minimum and measured from the compensator extinction position allows the calculation of the sample retardation R_S, given by[38]

$$R_S = -R_C \sin(2\theta_C), \tag{1}$$

where R_C is the compensator retardation and θ_C is the compensator angle. Equation (1) is valid only if the compensator retardation is greater than the sample retardation. When the sample retardation is greater, the roles of both wave plates are reversed, and the sample is rotated until an intensity minimum is obtained, in which case the sample retardation is computed using

$$R_S = -\frac{R_C}{\sin(2\theta_S)}. \tag{2}$$

A. Two-Wave-Plate System Analysis

The optical elements represented in Fig. 1 are considered to analyze the Brace–Köhler compensator method. Two wave plates producing, respectively, phase retardations ϕ_1 and ϕ_2 are placed between crossed polarizers. The orientations of their slow axes relative to the polarizer transmission direction are respectively θ_1 and θ_2. Jones calculus is used to determine the output intensity.[39] The various systems of axes for each optical element are represented in Fig. 2. The polarization transmission directions of the polarizer and the analyzer are respectively x_P and x_A, whereas the slow axes of wave plate 1 and wave plate 2 are respectively x_1 and x_2, as shown in Fig. 2.

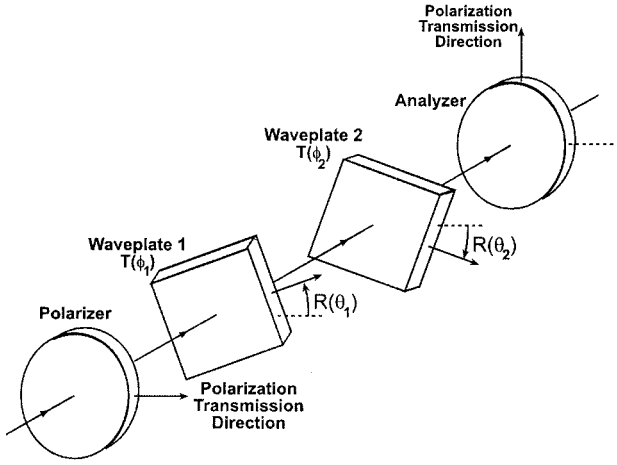

Fig. 1. Wave plate 1 and wave plate 2 with phase retardations equal to ϕ_1 and ϕ_2 are placed between crossed polarizers. Wave plate 1 and wave plate 2 slow-axis angles with respect to the first polarizer transmission direction are θ_1 and θ_2, respectively. The Jones rotation matrices are $R(\theta_1)$ and $R(\theta_2)$, respectively, and the Jones transmission matrices are $T(\phi_1)$ and $T(\phi_2)$.

The output light intensity is computed by calculating first the Jones vector $\boldsymbol{\varepsilon}_A$ in the system of the analyzer after traveling through the optical system,

$$\begin{aligned}\boldsymbol{\varepsilon}_A = &\begin{bmatrix} \sin\theta_2 & \cos\theta_2 \\ -\cos\theta_2 & \sin\theta_2 \end{bmatrix}\begin{bmatrix} 1 & 0 \\ 0 & \exp(j\phi_2) \end{bmatrix} \\ &\times \begin{bmatrix} \cos(\theta_2-\theta_1) & \sin(\theta_2-\theta_1) \\ -\sin(\theta_2-\theta_1) & \cos(\theta_2-\theta_1) \end{bmatrix}\begin{bmatrix} 1 & 0 \\ 0 & \exp(j\phi_1) \end{bmatrix} \\ &\times \begin{bmatrix} \cos\theta_1 & \sin\theta_1 \\ -\sin\theta_1 & \cos\theta_1 \end{bmatrix}\begin{pmatrix} 1 \\ 0 \end{pmatrix}. \end{aligned} \tag{3}$$

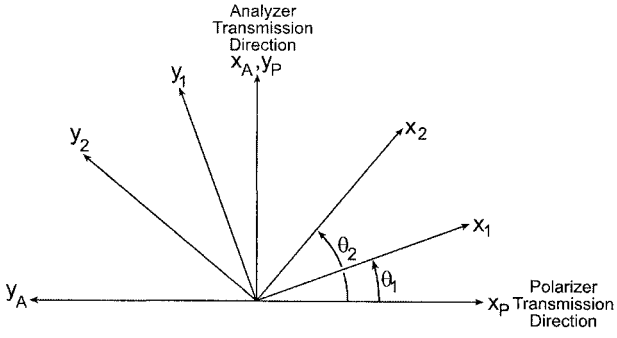

Fig. 2. Axes x_P and x_A are the polarization transmission direction of the polarizers. The wave plates' slow axes are x_1 and x_2, their fast axes are y_1 and y_2. The wave plates' slow-axes angles with respect to the polarizer transmission direction are θ_1 and θ_2.

In the Brace–Köhler case, wave plate 1 is at 45° from extinction. Performing the matrix multiplication, multiplying by the complex conjugate, and substituting $\theta_1 = 45°$, the relative intensity I_{BK} transmitted is

$$I_{BK\perp} = \sin^2 2\theta_2 \cos \phi_1 \sin^2 \frac{\phi_2}{2} + \frac{1}{2} \sin 2\theta_2 \sin \phi_1 \sin \phi_2 + \sin^2 \frac{\phi_1}{2}, \quad (4)$$

where the subscript $\perp$ indicates that the polarizers are crossed. A similar approach allows the derivation of the intensity between parallel polarizers by considering the Jones-vector component along the y_A axis of the analyzer system. The result is

$$I_{BK\parallel} = -\sin^2 2\theta_2 \cos \phi_1 \sin^2 \frac{\phi_2}{2} - \frac{1}{2} \sin 2\theta_2 \times \sin \phi_1 \sin \phi_2 + \cos^2 \frac{\phi_1}{2}. \quad (5)$$

Assuming no reflection or absorption in the optical system, both intensities satisfy

$$I_{BK\perp} + I_{BK\parallel} = 1. \quad (6)$$

The Brace–Köhler compensator retardation-measurement method assumes that the retardations of the sample and the compensator are small.[38] Under the small-retardation approximation, Eq. (4) becomes

$$I_{APX} = \left(\frac{\phi_1}{2} + \frac{\phi_2}{2} \sin 2\theta_2 \right)^2, \quad (7)$$

with I_{APX} representing the transmitted intensity. Under this approximation, a null of intensity is obtained when

$$\phi_1 = -\phi_2 \sin 2\theta_2. \quad (8)$$

The transmitted intensities calculated using Eqs. (4) and (7) are plotted in Fig. 3. The compensator phase retardation ϕ_2 corresponds to $\lambda/10$, which is the value of a commercially available Brace–Köhler compensator (model U-CBR1, manufactured by Olympus). The sample phase retardation ϕ_1 is arbitrarily chosen to correspond to $\lambda/18$. The exact expression for the transmittance, Eq. (4), shows that the minima observed in the Brace–Köhler method are not extinctions, as it is erroneously predicted by the small-retardation approximation, Eq. (7). The Brace–Köhler technique does not compensate completely for the phase retardation of the sample. Rotating the compensator between crossed polarizers only allows the total phase retardation between the electric field components along the polarizers' transmission directions to be minimized. It is therefore not strictly a compensation method.

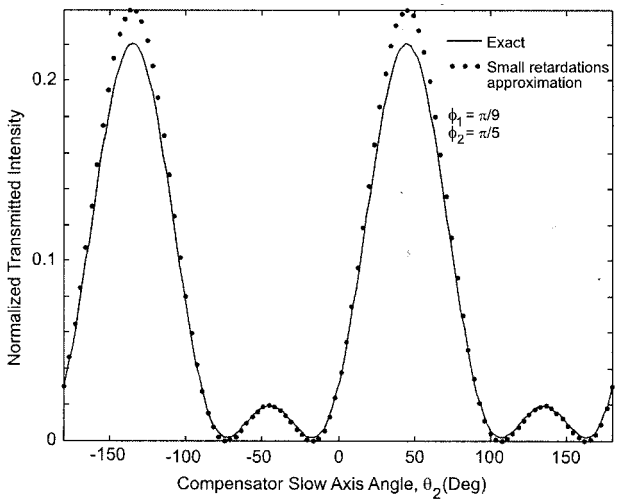

Fig. 3. In a two-wave-plate system, the first sample of phase retardation ϕ_1 corresponding to $\lambda/18$ is at 45° from extinction, and the compensator of phase retardation ϕ_2 corresponding to $\lambda/10$ is rotated. The intensity is plotted as a function of the compensator slow-axis angle θ_2. The solid curve represents the exact intensity; the dotted curve represents the intensity calculated using a small-retardation approximation.

B. Brace–Köhler Method Analysis

The first derivative of the intensity as a function of the rotating wave-plate orientation θ_2 is obtained from Eq. (4) as

$$\frac{\partial I_{BK}}{\partial \theta_2} = \cos 2\theta_2 [2 \sin 2\theta_2 \cos \phi_1 (1 - \cos \phi_2) + \sin \phi_1 \sin \phi_2]. \quad (9)$$

The locations of the extrema of intensity are given when $\partial I_{BK}/\partial \theta_2 = 0$. A first group of intensity extrema occurs for $\cos \theta_2 = 0$, i.e., $\theta_2 = (2n + 1) \times 45°$, where n is an integer. For the case represented in Fig. 3, these correspond to the global and local intensity maxima observed at $\pm 45°$ and $\pm 135°$. These intensity extrema, whether they are minima or maxima, are "nonretardation-based" extrema, as they are always observed for $\theta_2 = (2n + 1) \times 45°$ independently of the phase-retardation values ϕ_1 and ϕ_2. Substituting $\theta_2 = \pm 45°$ in Eq. (4), the normalized transmitted intensity of the nonretardation-based extrema is given as

$$I_{NRB}(\theta_2 = \pm 45°) = \sin^2 \left(\frac{\phi_1 \pm \phi_2}{2} \right). \quad (10)$$

A second group of intensity extrema occurs when the second factor in Eq. (9) equals zero. The analytical expression of the necessary angle θ_2 to produce these intensity extrema is given by

$$\sin 2\theta_2 = \frac{\sin \phi_1 \sin \phi_2}{2 \cos \phi_1 (\cos \phi_2 - 1)}. \quad (11)$$

This second group of extrema occurs only if

$$\left\| \frac{\sin \phi_1 \sin \phi_2}{2 \cos \phi_1 (\cos \phi_2 - 1)} \right\| \leqslant 1. \tag{12}$$

Provided the phase retardations ϕ_1 and ϕ_2 satisfy Eq. (12), four "retardation-based" intensity extrema occur, and their angular positions are given by

$$\begin{aligned} \sin(2\theta_2) &= \sin[2(\theta_2 + 180°)] = \sin[2(90° - \theta_2)] \\ &= \sin[2(-90° - \theta_2)]. \end{aligned} \tag{13}$$

In the case represented in Fig. 3, these extrema are intensity minima and occur for θ_2 equal to $-72.97°$, $-17.03°$, $107.03°$, and $162.97°$. Varying the angle θ_2 until these retardation-based extrema are observed, and knowing one wave-plate phase retardation ϕ_1 or ϕ_2, allows the determination of the other wave-plate phase retardation using Eq. (11). Equation (11) provides an exact expression for the calculation of the unknown retardation when using the Brace–Köhler compensator technique without restricting it to small retardations. It can therefore not only lead to more accurate retardation measurements, but also extend the range of compensator and sample retardations over which the Brace–Köhler compensator technique is applicable. Substituting Eq. (11) in Eq. (4), the normalized intensity of the retardation-based extrema is

$$I_{\mathrm{RB}} = \sin^2 \frac{\phi_1}{2} - \frac{\sin^2 \phi_1 \sin^2 \phi_2}{16 \cos \phi_1 \sin^2(\phi_2/2)}. \tag{14}$$

C. Brace–Köhler Method Applicability

The applicability condition of the technique can be stated simply as follows: For any given pair of sample and compensator retardations, retardation-based minima exist when one or the other plate is rotated. The condition of existence of the retardation-based minima can be expressed as one unique mathematical inequality by constraining their magnitude to be greater than zero and less than the nonretardation-based intensity extrema and is

$$0 \leqslant \sin^2 \frac{\phi_1}{2} - \frac{\sin^2 \phi_1 \sin^2 \phi_2}{16 \cos \phi_1 \sin^2 \dfrac{\phi_2}{2}} \leqslant \sin^2\left(\frac{\phi_1 + \phi_2}{2}\right). \tag{15}$$

This condition is represented in Fig. 4 as a function of sample and compensator retardations ranging from 0 to λ. The white region represents sample and compensator retardations for which the Brace–Köhler compensator technique cannot be applied to measure the sample retardation.

According to Eq. (6), whenever retardation-based maxima occur between crossed polarizers, then retardation-based minima occur between parallel polarizers and conversely, whenever retardation-based minima occur between crossed polarizers, retardation-based maxima occur between parallel polarizers. As a result, the Brace–Köhler compensator applicability

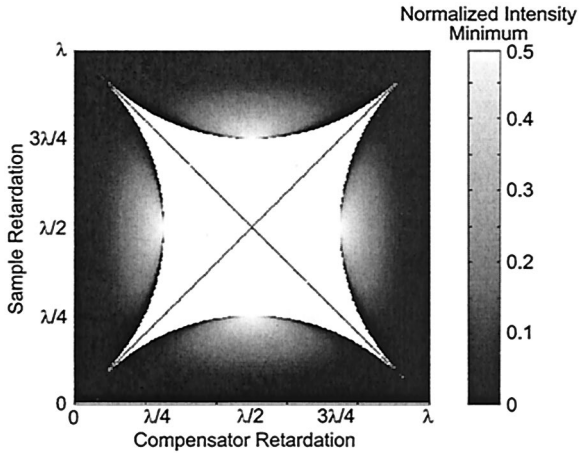

Fig. 4. Normalized intensity minima for Brace–Köhler compensator applicability range between crossed polarizers. The retardation-based intensity minima are calculated for sample and compensator retardations ranging from 0 to λ. It is assumed that the wave plates are between crossed polarizers. The white region represents retardations for which there are no retardation-based minima.

range may be increased by simply introducing the possibility of making the measurement between parallel polarizers.

The expressions for the retardation-based and nonretardation-based extrema between parallel polarizers are derived using Eqs. (6), (10), and (14) and are

$$I_{\mathrm{NRB}\|}(\theta_2 = \pm 45°) = \cos^2\left(\frac{\phi_1 \pm \phi_2}{2}\right), \tag{16}$$

$$I_{\mathrm{RB}\|} = \cos^2 \frac{\phi_1}{2} + \frac{\sin^2 \phi_1 \sin^2 \phi_2}{16 \cos \phi_1 \sin^2 \dfrac{\phi_2}{2}}. \tag{17}$$

Similar to the case between crossed polarizers, retardation-based minima between parallel polarizers exist whenever the inequality

$$0 \leqslant \cos^2 \frac{\phi_1}{2} + \frac{\sin^2 \phi_1 \sin^2 \phi_2}{16 \cos \phi_1 \sin^2 \dfrac{\phi_2}{2}} \leqslant \cos^2\left(\frac{\phi_1 + \phi_2}{2}\right) \tag{18}$$

is satisfied. The magnitude of the retardation-based minima between parallel polarizers is represented in Fig. 5 as a function of the sample and compensator retardations. The white region represents sample and compensator retardations for which the Brace–Köhler compensator technique cannot be applied between parallel polarizers.

By superimposing Figs. 4 and 5, sample and compensator retardations for which retardation-based minima can be observed and therefore the Brace–Köhler compensator technique applied are determined. This is shown in Figs. 6(a) and 6(b). The white region in Figs. 6(a) and 6(b) corresponds to

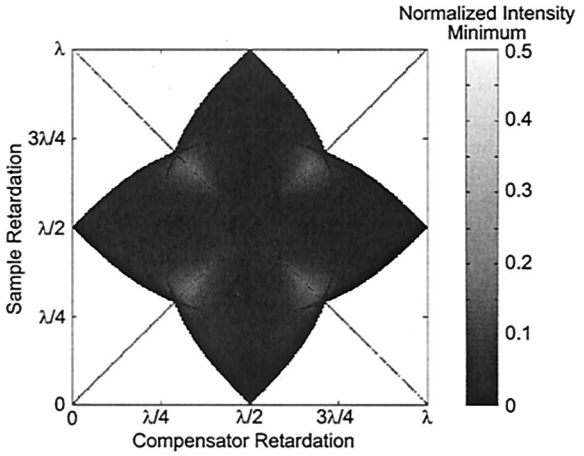

Fig. 5. Normalized intensity minima for Brace–Köhler compensator applicability range between parallel polarizers. The retardation-based intensity minima are calculated for sample and compensator retardations ranging from 0 to λ. It is assumed that the wave plates are between parallel polarizers. The white region represents retardations for which there are no retardation-based minima.

sample and compensator retardations producing no retardation-based minima.

D. Performance Characteristics

1. Resolvability Limit

Experimentally, only one intensity minimum needs to be found to determine the unknown retardation. The compensator model U-CBR1 manufactured by Olympus is rotatable from approximately $-50°$ to $+50°$. Over this range, two nonretardation-based maxima and one retardation-based minimum are observed. However, for a given phase retardation ϕ_2, there is a maximum phase retardation ϕ_1 beyond which Eq. (12) is not satisfied. This maximum value ϕ_{L1} can be computed with Eq. (12) by substituting $\theta_2 = 45°$:

$$\phi_{L1} = \arctan\left(2\,\frac{1-\cos\phi_2}{\sin\phi_2}\right). \tag{19}$$

For the retardation of the commercial Brace–Köhler compensator where ϕ_2 corresponds to $\lambda/10$, the maximum sample phase retardation ϕ_{L1} is approximately equal to $0.91715\phi_2$. The corresponding normalized transmitted intensity is calculated and represented as a function of the compensator orientation θ_2 in Fig. 7. The retardation-based minimum that occurred for the previous value of ϕ_1 between $\theta_2 = \pm 45°$ is not observed, and a minimum is now observed for $\theta_2 = -45°$. The applicability range of the Brace–Köhler compensator technique can be defined based on its ability to resolve the retardation-based intensity minimum from the closest nonretardation-based intensity maximum that occurs at $\theta_2 = \pm 45°$. This is illustrated in Fig. 8, where the transmitted intensity variations from the minimum intensity are plotted for various values of $\|\sin 2\theta_2\|$ as it approaches unity.

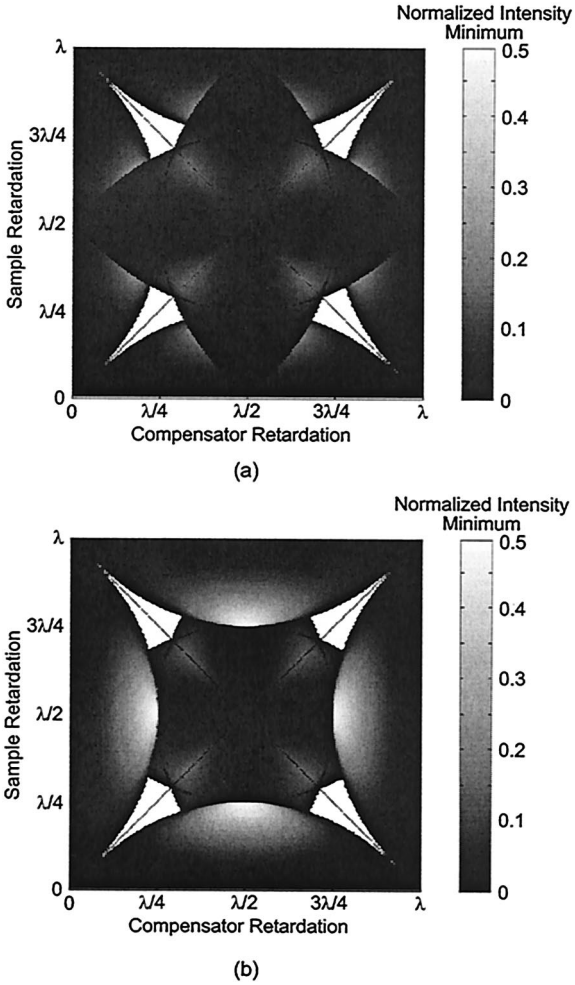

Fig. 6. Retardation-based minima between crossed and parallel polarizers: (a) Retardation based minima between parallel polarizers are superimposed onto those between crossed polarizers. (b) Retardation-based minima between crossed polarizers are superimposed onto those between parallel polarizers.

The rotating wave-plate phase retardation ϕ_2 corresponds to $\lambda/10$. The sample phase retardation is calculated for various values of $\|\sin 2\theta_2\|$ using Eq. (11). The successive values of $\|\sin 2\theta_2\|$ are indicated on each plot. To determine the value of $\|\sin 2\theta_2\|$ for which the retardation-based intensity minimum cannot be resolved, the intensity variations from the intensity minimum are plotted as a function of the compensator orientation θ_2. To generate the plots in Fig. 8, it is assumed that the power of the light incident upon the first polarizer is 15 mW, which corresponds to the power of a Spectra Physics model 120S He–Ne laser. The resolvability limit of the technique can be defined as the smallest intensity variation between a minimum and an adjacent maximum that can be detected by the photodetector. For a minimum measurable intensity variation of approximately 1 nW, the intensity minimum is resolvable for $\|\sin 2\theta_2\|$ equal to 0.9977, 0.9981, and 0.9991, respectively, in Figs. 8(a), 8(b), and 8(c). However, the minimum is not resolvable for $\|\sin 2\theta_2\|$ equal to

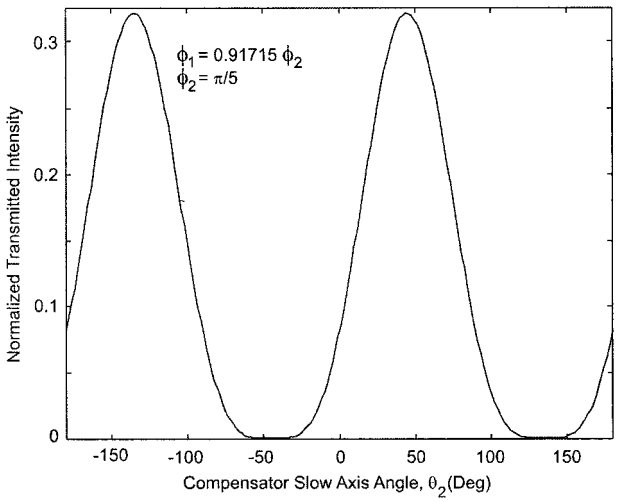

Fig. 7. Normalized transmitted intensity for the limiting case for the existence of retardation-based minima. Shown is the compensator phase retardation ϕ_2 corresponding to $\lambda/10$. The retardation limit of the sample is calculated using Eq. (11) with θ_2 equal to $-45°$. For this limiting case, the retardation-based intensity minimum merges with the nonretardation-based maximum at $-45°$.

0.9998 in Fig. 8(d). As a result, the limit of applicability of the Brace–Köhler compensator technique is mathematically given by

$$\left\| \frac{\sin \phi_1 \sin \phi_2}{2 \cos \phi_1(\cos \phi_2 - 1)} \right\| < 0.999, \qquad (20)$$

for a minimum measurable intensity variation of 1 nW.

2. *Resolution*

The resolution is defined as the smallest retardation change measurable. It depends on several parameters, such as the angular resolution of the rotating mount in which the compensator is placed, the compensator retardation, and the sample retardation. For a given compensator retardation, the resolution can be calculated as a function of the angular resolution and the sample retardation. Considering a compensator and a sample with phase retardations ϕ_c and ϕ_{s1}, the compensator angle θ_c at which the intensity minimum is measured is given by Eq. (11) as

$$\sin(2\theta_c) = \frac{\sin \phi_{s1} \sin \phi_c}{2 \cos \phi_{s1}(\cos \phi_c - 1)}. \qquad (21)$$

Considering the angular resolution $\Delta\theta$, the nearest measurable sample phase retardation ϕ_{s2} is given by

$$\tan \phi_{s2} = \frac{2(\cos \phi_c - 1)\sin(2\theta_c + 2\Delta\theta)}{\sin \phi_c}. \qquad (22)$$

The difference between ϕ_{s2} and ϕ_{s1} defines the resolution. The resolution is calculated and represented as a function of sample retardation and angular resolution in Figs. 9(a) and 9(b). Two different compensator retardations, respectively, $\lambda/10$ and $\lambda/30$, are considered that correspond to two commercially available Brace–Köhler compensators. The maximum resolution is approximately 0.2 nm and 0.1 nm, respectively, for a 0.1° angular resolution. The resolution can be improved by decreasing the angular resolution of the rotating dial. An angular resolution of 0.01° allows resolutions of 0.04 nm and 0.02 nm to be obtained. This is comparable to the resolution obtained with the commercially available photoelastic instrument (Exicor model 150AT manufactured by Hinds Instruments[34,40–42]).

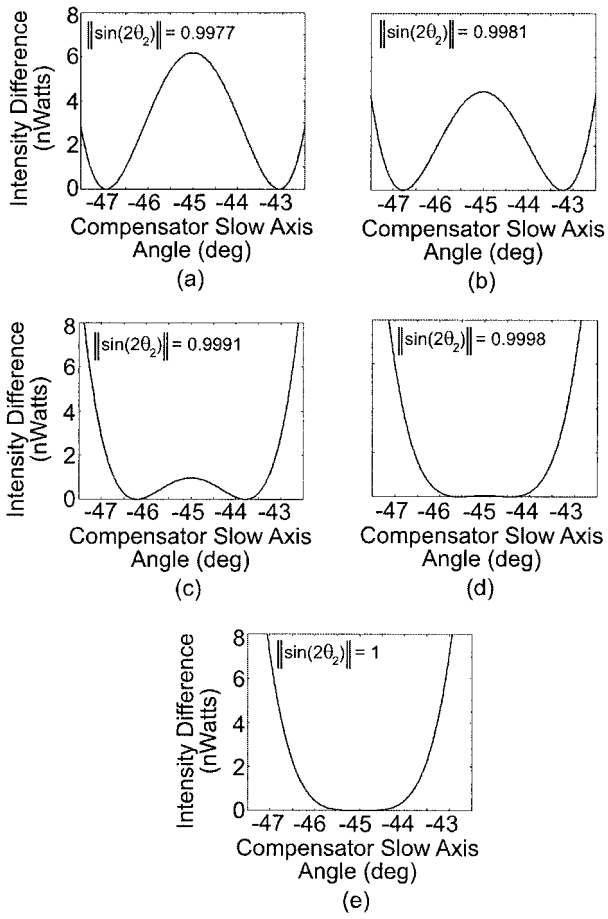

Fig. 8. Resolvability of the Brace–Köhler compensator technique. (a)–(e) Transmitted intensity for various values of sample phase retardation ϕ_1. The compensator phase retardation ϕ_2 corresponds to $\lambda/10$. The input intensity is equal to 15 mW.

E. Low-Level Retardation-Measurement Error

The measurement error of the Brace–Köhler compensator method is calculated taking into account the small-retardation approximation and the angular uncertainty of the measurement. For a given pair of sample and compensator, the exact angle producing a minimum of intensity is calculated using Eq. (11). The angular uncertainty of the measurement is defined as the range of angles over which the intensity variation is less than the minimum measurable intensity change. The retardation is calculated at the ends of the angular range using the small-

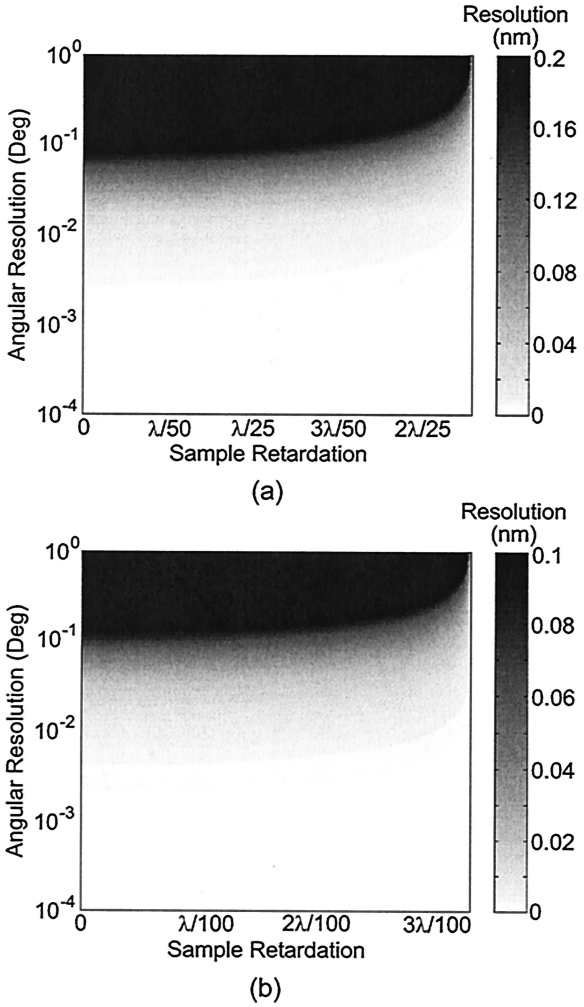

Fig. 9. Resolution of the Brace–Köhler compensator technique as a function of sample retardation and angular resolution. (a) Compensator retardation equals λ/10. (b) Compensator retardation equals λ/30.

retardation approximation, Eq. (1). The relative measurement error is then computed by expressing the maximum retardation deviation as a percentage of the sample's true retardation.

The measurement error is calculated and presented for the Brace–Köhler compensator in Fig. 10 for sample and compensator retardations between 0 and λ/8. Only 22.125% of the total number of error data used to generate Fig. 10 are less than 1%. The error increases as sample and compensator retardations increase owing to the small-retardation approximation that predominates over the error from the uncertainty in the angle measurement. It also increases as sample and compensator retardations become very small owing predominantly to the uncertainty of the angle measurement. More precisely, it increases beyond 10% for retardations less than λ/500. At that very low level of retardation, the absolute uncertainty of the measurement is not greater than that at larger retardations; however, it becomes relatively large compared with the retardation to be measured.

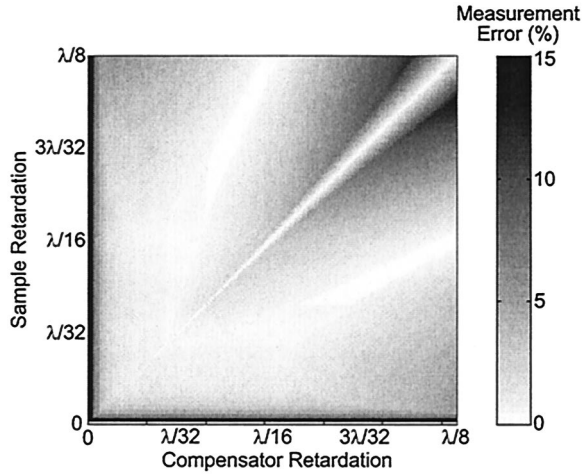

Fig. 10. Error in Brace–Köhler compensator method for sample and compensator retardations ranging from 0 to λ/8. The error is determined taking into account the measurement angular uncertainty that is due to the sensitivity of the detector and taking into account the small-retardation approximation. Only 22.125% of the total number of error data in the plot are <1%.

3. Two-Wave-Plate Compensator

The Brace–Köhler technique has numerous shortcomings that limit its applicability range and its accuracy. It is not a rigorous compensation method and does not produce extinction as is the case, for example, with the Sénarmont compensator technique.[38] In a two-wave-plate system, there exists a relative orientation of the wave plates resulting in a total retardation equal to 0 or λ, producing a linearly polarized output. If this linearly polarized output exists, it is not parallel to the analyzer transmission direction, and extinction can be obtained only if the analyzer is rotated so as to be perpendicular to the linearly polarized electric field exiting the second wave plate. This is the basis for the development of a new retardation-measurement technique, the two-wave-plate compensator (TWC) technique.[43]

A. Two-Wave-Plate System Analysis

An analytical expression of the rotating wave-plate angle necessary to obtain a linearly polarized output is needed. This can be done using Jones calculus as was done in Section 2. The Jones vector expressed in the system of axes associated with the second wave plate is given by

$$\boldsymbol{\varepsilon}_2 = T(\phi_2)R(\theta_2)\begin{pmatrix} a \\ b\ \exp\left(j\,\frac{\pi}{2}\right) \end{pmatrix}, \tag{23}$$

where $T(\phi_2)$ is the transmission matrix of phase retardation ϕ_2, $R(\theta_2)$ is the rotation matrix of angle θ_2, and a and b are the components' magnitudes of the Jones-vector characteristic of the electric field exiting the first wave plate expressed in the system of axes of the crossed polarizers. It can be shown that the major and minor axes of the ellipse traced by the electric field exiting the first wave plate are given by a =

$\cos(\phi_1/2)$ and $b = -\sin(\phi_1/2)$. Substituting into Eq. (23) and carrying out the matrix multiplication, $\boldsymbol{\varepsilon}_2$ can be written in the form

$$\boldsymbol{\varepsilon}_2 = \begin{pmatrix} a_1 \exp(j\delta_1) \\ a_2 \exp[j(\delta_2 + \phi_2)] \end{pmatrix}, \tag{24}$$

with

$$a_1 = (a^2 \cos^2 \theta_2 + b^2 \sin^2 \theta_2)^{1/2}, \tag{25}$$

$$a_2 = (a^2 \sin^2 \theta_2 + b^2 \cos^2 \theta_2)^{1/2}, \tag{26}$$

$$\delta_1 = \arctan\left(\frac{b \sin \theta_2}{a \cos \theta_2}\right), \tag{27}$$

$$\delta_2 = \arctan\left(\frac{b \cos \theta_2}{-a \sin \theta_2}\right). \tag{28}$$

The condition for the electric field to be linearly polarized is given by

$$\delta_2 + \phi_2 = \delta_1 + k\pi, \tag{29}$$

where k is an integer. Substituting the expressions of δ_1 and δ_2 in Eq. (29) and using trigonometric identities leads to the TWC formula for linearly polarized output as

$$\sin 2\theta_2 = -\frac{\tan \phi_1}{\tan \phi_2}. \tag{30}$$

B. Two-Wave-Plate Compensator Applicability

The condition of existence of the angle θ_2 in Eq. (30) is given by

$$\left\| -\frac{\tan \phi_1}{\tan \phi_2} \right\| \leqslant 1. \tag{31}$$

Equation (31) allows one to determine which of the sample or compensator waveplates is to be rotated to obtain linearly polarized light. Contrary to the Brace–Köhler compensator technique, the TWC technique is guaranteed to produce linearly polarized output provided Eq. (31) is satisfied. The applicability range of the TWC technique can be represented using Eq. (31) as a function of the sample and compensator retardations. Figure 11 represents the magnitude of the angle θ_2 in degrees for various sample and compensator retardations. The angle θ_2 is calculated using Eq. (30). Depending on the retardation values, either the compensator needs to be rotated to obtain linearly polarized light, which is represented in Fig. 11(a), or the sample needs to be rotated, which is represented in Fig. 11(b). A linearly polarized output can always be obtained, provided the fixed and rotating wave-plate roles are assigned so that Eq. (31) is satisfied. If, by rotating the compensator (or the sample), Eq. (31) is not satisfied, i.e., $\|\sin 2\theta_2\| > 1$, it is obvious that rotating the sample (or the compensator) then satisfies Eq. (31), since reversing the roles of the two wave plates results in inverting the ratio $\tan \phi_1/\tan \phi_2$.

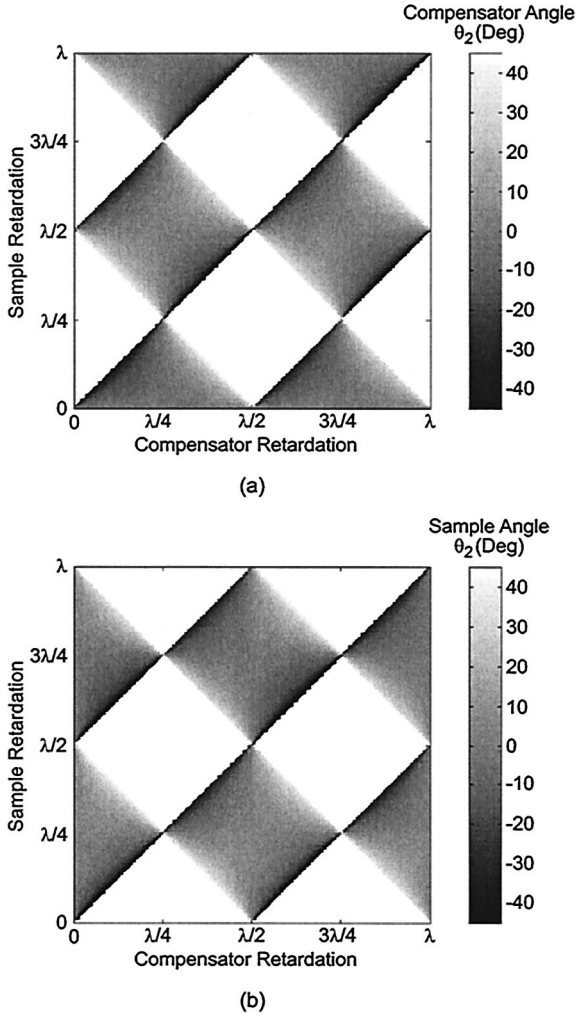

Fig. 11. Magnitude of the angle θ_2 producing linearly polarized light is calculated for sample and compensator retardations ranging from 0 to λ. (a) The linearly polarizing angle is calculated when the compensator is rotated. The white region represents retardations for which no linearly polarized output is produced as the compensator is rotated. (b) The linearly polarizing angle is calculated when the sample is rotated. The white region represents retardations for which no linearly polarized output is produced as the sample is rotated.

C. Two-Wave-Plate Compensator Working Principle

A detailed study of the output light polarization is shown in Figs. 12, 13, 14, and 15 for a sample of phase retardation corresponding to 0.15λ and a compensator of phase retardation corresponding to 0.45λ. The x axis of the system in which the polarization states are plotted in Figs. 13 and 15 corresponds to the first polarizer transmission direction. For the retardations used in this example, a linearly polarized output is produced when the sample of retardation 0.15λ is rotated. Using Eq. (30), the sample orientation producing a linearly polarized output is calculated and is equal to 6.83°. The lengths of the semiaxes and the ellipticity of the output light polarization ellipse as a function of the sample orientation are plotted in Fig. 12. The linearly polarized output is

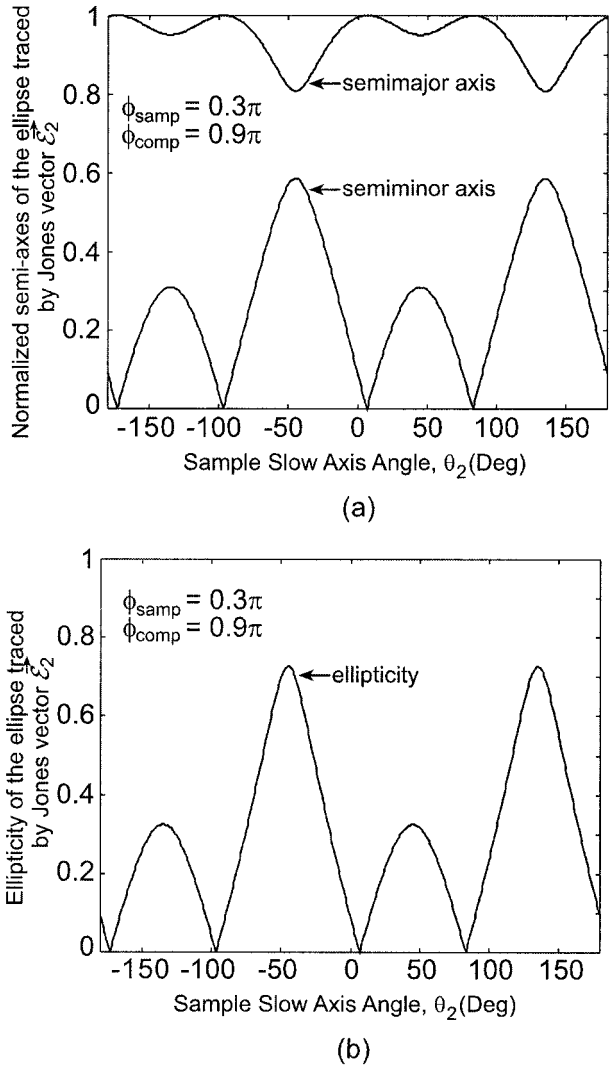

Fig. 12. Semiminor, semimajor axes, and the ellipticity of the output light are plotted as a function of the sample slow-axis angle.

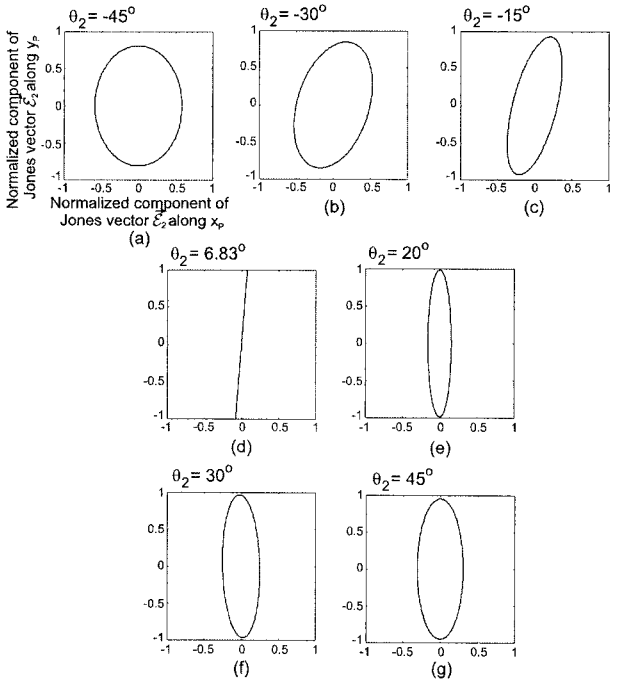

Fig. 13. Output light polarization states are represented for various sample slow-axes angles in the polarizer system of axes x_P and y_P (Fig. 2). The sample phase retardation ϕ_{samp} corresponds to 0.15λ, and the compensator phase retardation ϕ_{comp} corresponds to 0.45λ. Linearly polarized light is produced for a sample slow-axis angle equal to 6.83°.

produced when the semiminor axis of the polarization ellipse is equal to zero. In Fig. 13, the output light polarization is represented when the sample of retardation 0.15λ is rotated from −45° to +45°. As calculated, the linearly polarized output is produced for θ_2 equal to 6.83°, which is also seen in Fig. 12. By incrementally rotating the analyzer so that its transmission direction is always parallel to the semiminor axis of the polarization ellipse as the linearly polarizing wave plate is rotated, the intensity transmitted goes through extinction when the semiminor axis goes through zero.

In contrast, Figs. 14 and 15 represent the semiaxes, ellipticity, and polarization states as the compensator is rotated. In this configuration, the nonlinearly polarizing wave plate is rotated, and no linearly polarized output is produced between −45° and +45°. The semiminor axis of the output polarization ellipse decreases monotonically. The semiaxes lengths, minor semiaxis orientation, and ellipticity of the polarization states represented in Figs. 13 and 15 are summarized in Tables 1 and 2.

The observation of the output polarization states as the linearly polarizing or the nonlinearly-polarizing wave plate is rotated allows one to develop the experimental procedure needed to determine whether the sample or the compensator has to be rotated to use the TWC technique. The polarizers are first crossed. One of the wave plates, compensator or sample, is rotated at 45° from extinction and is chosen to be the fixed wave plate in this test experiment. The other wave plate, sample or compensator, is rotated so it is at ±45° from extinction and is chosen to be the rotating wave plate. With the wave plates in their respective initial orientations, the intensities transmitted between crossed and parallel polarizers are determined by rotating the analyzer accordingly. The analyzer must then be oriented to either of the positions that produced the minimum intensity ensuring the analyzer transmission direction is parallel to the semiminor axis of the output light polarization ellipse. The rotating wave plate is rotated by increments from ±45° to ∓45°. For each rotating waveplate orientation, the analyzer is rotated so a minimum of intensity is transmitted, ensuring the analyzer transmission direction is locked on the semiminor axis of the output polarization ellipse. The intensity transmitted through the analyzer is observed as it is rotated. If the intensity goes through extinction, the wave plate that is initially

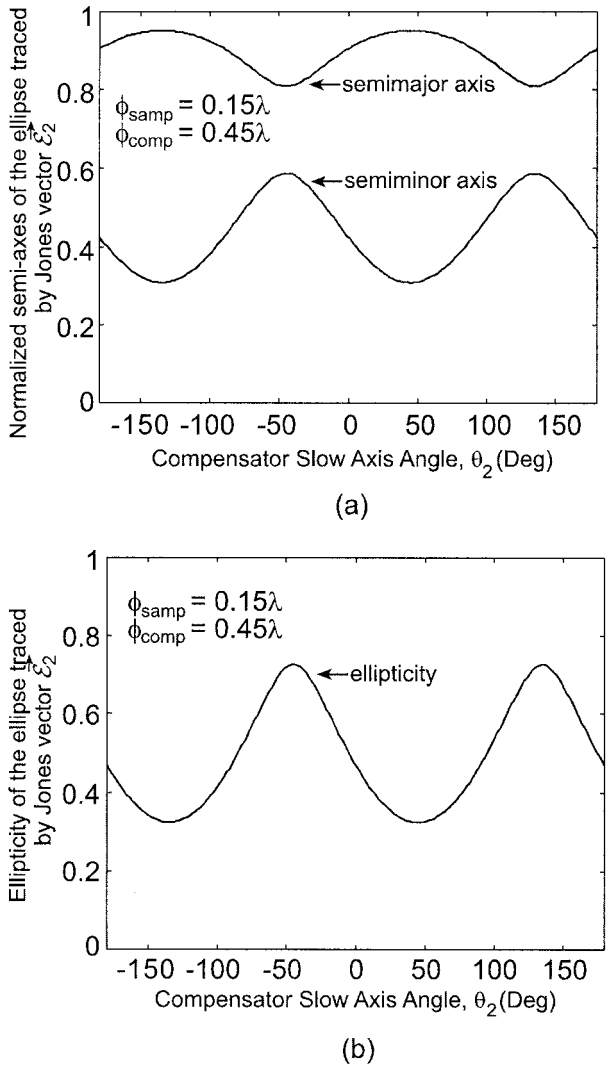

Fig. 14. Semiminor, semimajor axes, and the ellipticity of the output light are plotted as a function of the compensator slow-axis angle.

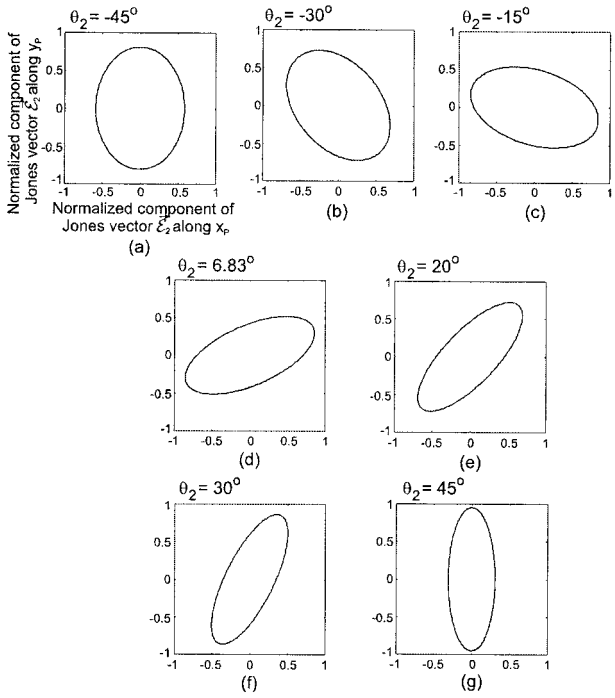

Fig. 15. Output light polarization states are represented for various compensator slow-axes angles in the polarizer system of axes x_P and y_P (Fig. 2). The sample phase retardation ϕ_{samp} corresponds to 0.15λ, and the compensator phase retardation ϕ_{comp} corresponds to 0.45λ. No linearly polarized light is produced when the compensator is rotated.

chosen as the rotating wave plate is the linearly polarizing wave plate. Consequently, the measurement using the TWC technique is to be done by rotating the same wave plate. By contrast, if the intensity decreased or increased monotonically during the test experiment, the wave plate that is initially chosen as the rotating wave plate is the nonlinearly polarizing wave plate. This wave plate must therefore be oriented at 45° from extinction and be fixed to use the TWC technique, while the other wave plate must be rotated. This experimental procedure is illustrated in Fig. 16.

The measurement using the TWC technique consists of following the steps in the procedure represented in the flow chart of Fig. 17. Once the test experiment has been run, the phase-retardation values of the sample ϕ_{samp} and that of the compensator ϕ_{comp} are assigned to ϕ_1 or ϕ_2, depending upon which is the linearly polarizing wave plate. Following the determination of the wave plates' roles, the analyzer transmission direction must be brought parallel to the semiminor axis of the output polarization ellipse by placing the rotating wave plate at ±45° from extinction and setting the analyzer to produce a minimum of intensity. This is similar to what is done in the test experiment. Having set the analyzer transmission direction parallel to the semiminor axis of the polarization ellipse, the rotating wave plate is rotated by small increments, and the analyzer is rotated at each increment so the intensity transmitted is minimum. When extinction is produced, the rotating wave-plate angle θ_e is recorded and is used to determine the unknown sample retardation. Equation (30) is used to calculate the unknown ϕ_{samp}. Two different expressions are derived to calculate the sample retardation depending if $\phi_1 = \phi_{samp}$ or $\phi_1 = \phi_{comp}$. These expressions are indicated at the end branches of the flow chart.

D. Performance Characteristics

1. Resolvability Limit

The applicability of the TWC technique for measuring retardation depends upon the capability of the optical system to resolve the point of extinction from the adjacent local maximum occurring for θ_2 equal to ±45° (Fig. 12). As the tangents of the sample and compensator retardations converge toward the same value, the angle producing linearly polarized light approaches ±45°, and the adjacent maximum inten-

Table 1. Semiaxes Lengths, Ellipticity, and Semiminor Axis Angle of the Output Light Polarization Ellipse as a Function of the Sample Slow-Axis Angle θ_2[a]

θ_2 (deg)	Semiminor axis normalized	Semiminor axis angle (deg)	Semimajor axis normalized	Ellipticity
−45	0.5878	0	0.8090	0.7265
−30	0.4847	−16.89	0.8746	0.5542
−15	0.2965	−13.97	0.9550	0.3105
6.83	0	−4.40	1.0000	0
20	0.1585	0.05	0.9874	0.1605
30	0.2503	1.47	0.9682	0.2585
45	0.3090	0	0.9510	0.3249

[a] $\phi_{samp} = 0.3\pi$, $\phi_{comp} = 0.9\pi$.

sity decreases, which renders more difficult the distinction between the extinction and the adjacent maximum. This is illustrated in Fig. 18, where the intensity transmitted along the semiminor axis of the output light polarization ellipse is plotted as a function of the rotating wave-plate angle between −48° and −42° for a light source power I_o equal to 15 mW. The retardations of the sample and compensator are respectively equal to 0.15λ and 0.1502λ. In the case where the compensator is the rotating wave plate, a linearly polarized output is produced for θ_2 equal to −47.08°, −42.91°, 132.92°, and 137.08°. When the compensator is rotated between −48° and −42°, extinction is produced for two of these angles, shown in Fig. 18. Also shown in Fig. 18 is the intensity transmitted as the sample is rotated over the same angular range. When the sample is rotated from −45° to +45°, no linearly polarized output is produced, and the semiminor axis of the output polarization ellipse increases monotonically similarly to that shown in Fig. 14. It will be shown analytically that the intensity of the minimum produced at −45° when the sample is rotated is equal to that of the local maximum produced when the compensator is rotated. This is seen in Fig. 18. The capability of the system for measuring the intensity difference between the intensity of the global minimum occurring at ±45° when the nonlinearly polarizing wave plate is rotated and the intensity of the global minimum occurring when the linearly polarizing wave plate is rotated defines the resolvability limit of the TWC technique. This depends upon the sensitivity of the system in measuring and resolving low-level intensities. In the example of Fig. 18, the minimum measurable intensity must be less than 5 nW in order to resolve the global minimum when the compensator is rotated and the global minimum when the sample is rotated.

The intensity along the semiaxes of the output polarization ellipse is computed using Eqs. (42) and (43) that are derived in the appendix section. The result is

$$I_1(\theta_2 = \pm 45°) = I_o \cos\left(\frac{\phi_1 \pm \phi_2}{2}\right)^2, \tag{32}$$

$$I_2(\theta_2 = \pm 45°) = I_o \sin\left(\frac{\phi_1 \pm \phi_2}{2}\right)^2. \tag{33}$$

In Fig. 18, in order for the local maximum occurring for θ_2 equal to −45° to be resolved, its intensity must be greater than the minimum intensity I_{min} measurable by the experimental system. This condition is expressed as

$$I_o \cos\left(\frac{\phi_1 \pm \phi_2}{2}\right)^2 > I_{min}, \tag{34}$$

$$I_o \sin\left(\frac{\phi_1 \pm \phi_2}{2}\right)^2 > I_{min}. \tag{35}$$

Using the equations above, the resolvability condition can be stated as a function of sample and com-

Table 2. Semiaxes Lengths, Ellipticity, and Semiminor Axis Angle of the Output Light Polarization Ellipse as a Function of the Compensator Slow-Axis Angle θ_2[a]

θ_2 (deg)	Semiminor axis normalized	Semiminor axis angle (deg)	Semimajor axis normalized	Ellipticity
−45	0.5878	0	0.8090	0.7265
−30	0.5587	40.73	0.8294	0.6736
−15	0.4950	73.34	0.8687	0.5697
6.83	0.3955	113.71	0.9184	0.4306
20	0.3481	136.77	0.9374	0.3713
30	0.3234	154.09	0.9462	0.3418
45	0.3090	180	0.9510	0.3249

[a] $\phi_{samp} = 0.3\pi$, $\phi_{comp} = 0.9\pi$.

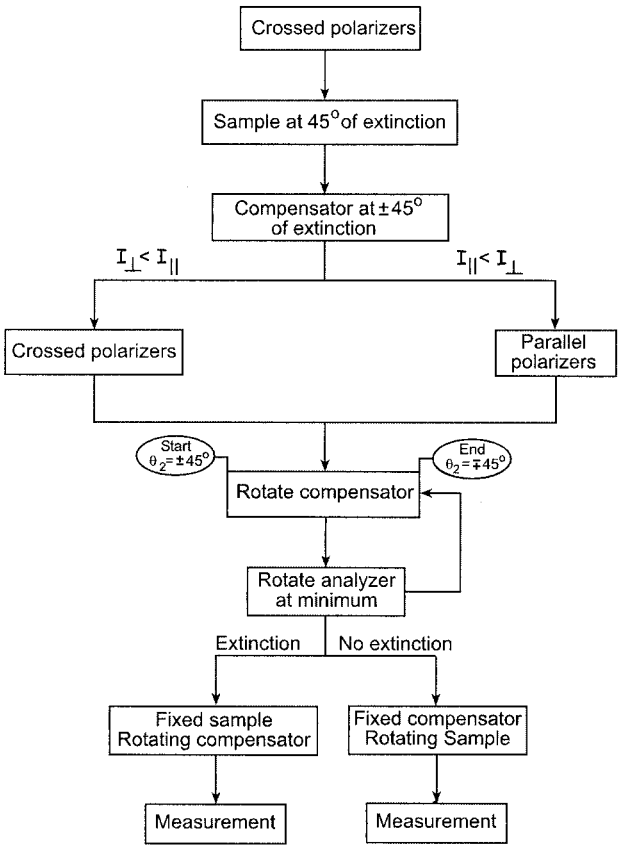

Fig. 16. Flow chart representing the experimental procedure to determine whether the sample or the compensator needs to be rotated to produce linearly polarized light. The flow chart is based on having the analyzer transmission direction parallel to the output ellipse semiminor axis. Sample (compensator) and analyzer are successively rotated to observe the variations of the transmitted intensity.

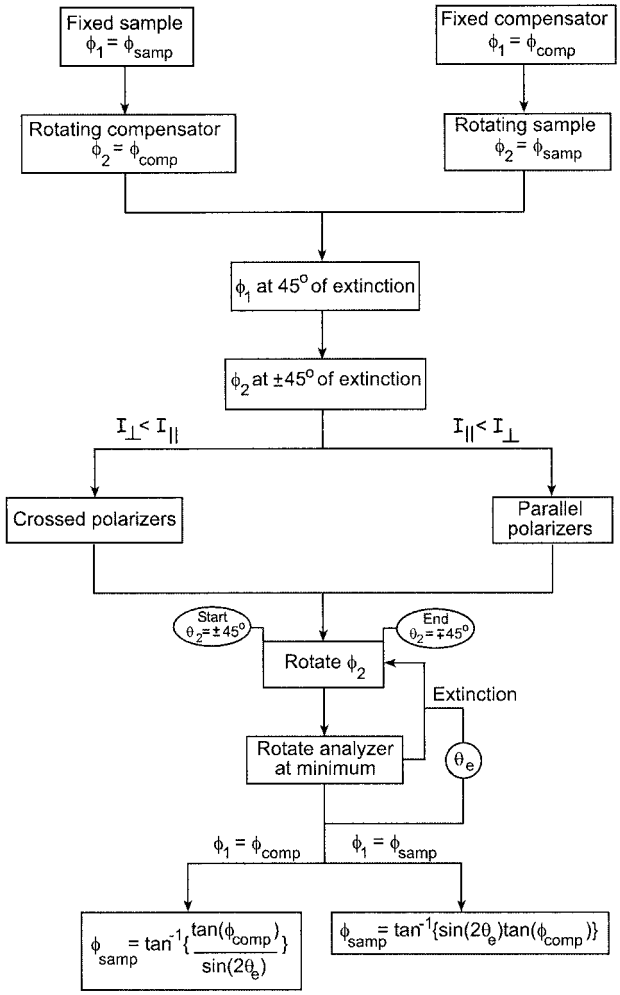

Fig. 17. Flow chart representing the experimental procedure to measure retardation using the TWC method.

pensator retardations, the input power, and the minimum measurable power, as

$$2 \arcsin\left(\sqrt{\frac{I_{\min}}{I_o}}\right) < \phi_1 - \phi_2 < 2 \arccos\left(\sqrt{\frac{I_{\min}}{I_o}}\right), \quad (36)$$

$$2 \arcsin\left(\sqrt{\frac{I_{\min}}{I_o}}\right) < \phi_1 + \phi_2 < 2 \arccos\left(\sqrt{\frac{I_{\min}}{I_o}}\right). \quad (37)$$

2. Resolution

The resolution of the TWC technique can be quantified as a function of the sample retardation and angular resolution as was done with the Brace–Köhler compensator. The compensator angle θ_c necessary to produce linearly polarized light is given by Eq. (30) as $\sin(2\theta_c) = -\tan \phi_{s1}/\tan \phi_c$, with ϕ_{s1} and ϕ_c being the sample and compensator phase retardations. The nearest measurable retardation ϕ_{s2} is given by

$$\tan \phi_{s2} = -\tan \phi_c \sin(2\theta_c + 2\Delta\theta), \quad (38)$$

with $\Delta\theta$ the angular resolution. The difference between ϕ_{s2} and ϕ_{s1} allows the resolution to be computed. The TWC resolution is calculated and represented as a function of the sample retardation and the angular resolution in Figs. 19(a) and 19(b) for compensator retardations $\lambda/10$ and $\lambda/30$, respectively. The TWC resolution is comparable to that of the Brace–Köhler compensator technique and is ~0.1 nm and ~0.2 nm, respectively, for an angular resolution of 0.1°. Similarly to the Brace–Köhler compensator technique, the TWC resolution improves with angular resolution. For an angular resolution of 0.01°, resolutions of 0.04 nm and 0.02 nm are achieved, respectively.

E. Measurement Error

The measurement error using the TWC is calculated by determining the angular measurement uncertainty, which is defined as the angular range over which the output light intensity decreases beyond the minimum measurable intensity. The corresponding measured retardations at either extreme of the angular range are calculated using the TWC formula and compared with the true sample retardation. Figure 20 represents the relative measurement error

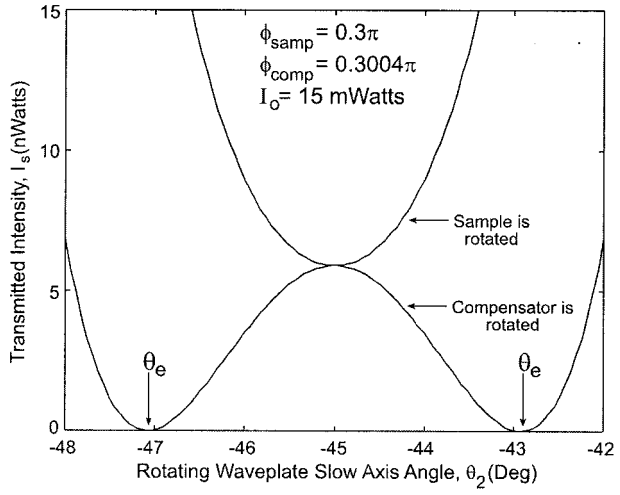

Fig. 18. Intensity transmitted along the analyzer transmission direction is plotted for a sample phase retardation corresponding to 0.15λ and a compensator phase retardation corresponding to 0.1502λ. The input intensity is 15 mW. In one case, the sample is rotated and no extinction is obtained (upper curve with one global minimum). In the other case, the compensator is rotated and extinction is obtained (lower curve with two global minima and one local maximum).

for sample and compensator retardations ranging from 0 to λ. A minimum measurable intensity of 5 nW is considered to plot Fig. 20. The relative error of the measurement remains <2% over the entire range of sample and compensator retardations except when the compensator retardation is a multiple of a quarter-wave plate or a half-wave plate, in which case the error increases beyond 10%. The error remains low, however, when the sample retardation is a multiple of a quarter-wave plate or a half-wave plate.

The measurement error of the TWC technique is also calculated for retardations between 0 and λ/8 and is represented in Fig. 21. In this plot, 71.41% of the total number of error data are less than 1%, whereas only 22.125% of the error data was less than 1% in the Brace–Köhler compensator case in Fig. 10 in Section 2. This shows that even for smaller retardations, the TWC technique is more accurate than the Brace–Köhler compensator technique. The TWC error shown in Fig. 21 is entirely due to the angular uncertainty of the measurement. Therefore, as the retardations increase, the relative error decreases, as there are no small-retardation approximations. However, as retardations become very small, the relative error increases. As in the case of the Brace–Köhler compensator, it increases beyond 10% for retardations less than λ/500, and this is also because the error from the angular uncertainty becomes relatively large.

4. Experiments

The TWC technique is compared experimentally with the Brace–Köhler and Sénarmont techniques using the configuration in Fig. 22. A He–Ne laser of out-

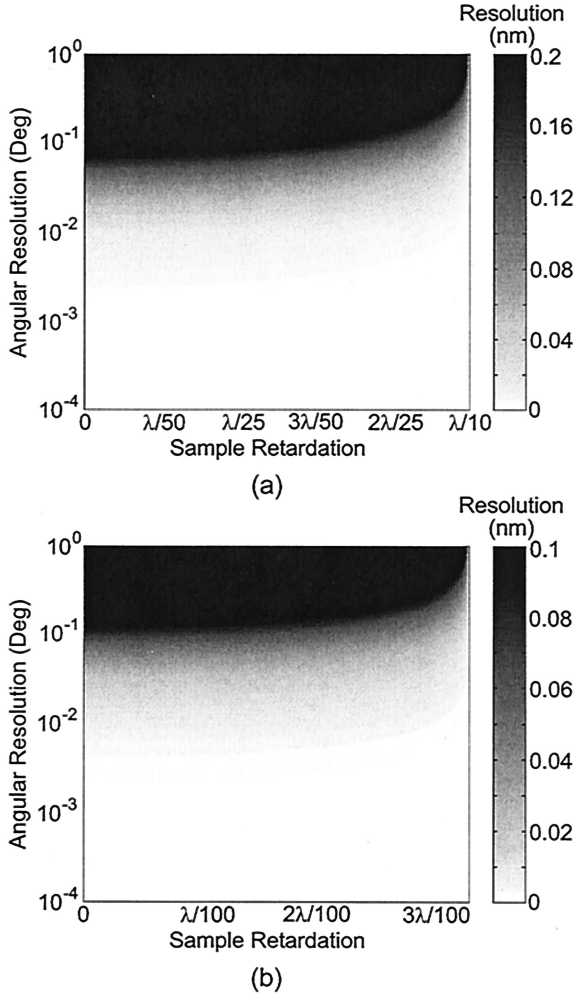

Fig. 19. Resolution of the TWC technique as a function of sample retardation and angular resolution. (a) Compensator retardation equals λ/10. (b) Compensator retardation equals λ/30.

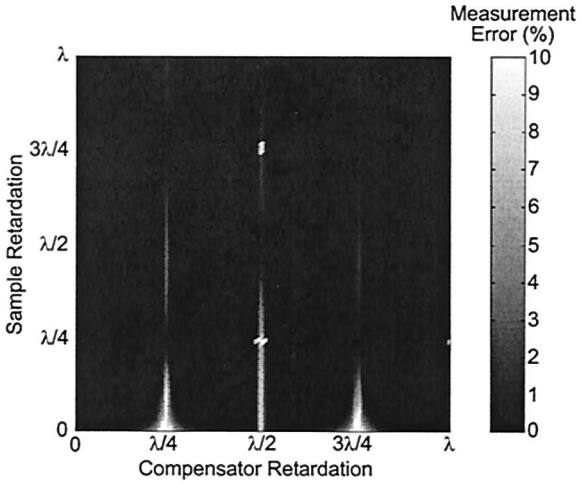

Fig. 20. Measurement error in TWC for any given pair of sample and compensator retardations. The error is calculated based on the measurement angular uncertainty owing to the sensitivity limit of the experiment.

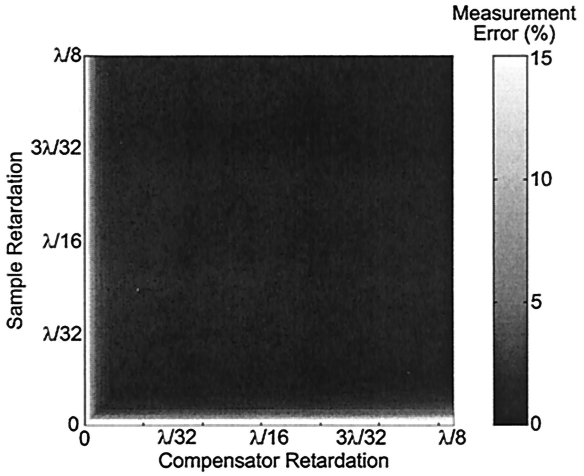

Fig. 21. Error in TWC method for sample and compensator retardations ranging from 0 to λ/8. The error is determined taking into account the measurement angular uncertainty owing to the sensitivity of the detector. 71.41% of the total number of error data in the plot are <1%.

put power equal to 15 mW is used as a light source. The polarizers P and A are Glan–Thompson prisms. The extinction ratio of the polarizers is measured before the retardation measurements and is equal to 6.6×10^{-8}. For the TWC and Brace–Köhler techniques, the compensator C is the Brace–Köhler compensator model U-CBR1 of retardation equal to 59.66 nm at the wavelength of 546.1 nm. It is placed in a rotating dial, allowing the compensator to rotate from −50° to +50°. It is usually supplied for use in a polarization microscope to measure retardations less than λ/30. For the Sénarmont compensator technique, a quarter-wave plate designed for 632.8 nm is placed at extinction after the sample. Having placed the sample at 45° from extinction, the output light exiting the quarter-wave plate is linearly polarized. Extinction is obtained by rotating the analyzer perpendicular to the electric field. It can be shown that the analyzer angle producing extinction is exactly half the phase shift of the sample. The Sénarmont compensator method is a widely used technique, and more details can be found in the literature.[38] Two samples are used to compare the methods. Manufacturing wave plates of small retardations is difficult and may not be as accurate as

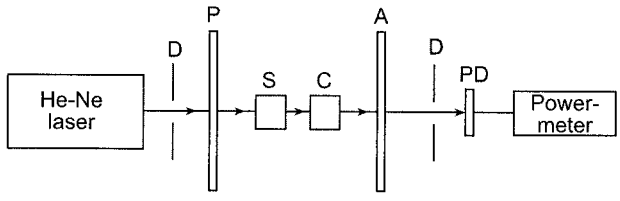

Fig. 22. Experimental configuration used to measure small retardations with the TWC, the Brace–Köhler compensator, and the Sénarmont compensator techniques. The light source is a He–Ne laser: D, diaphragm; P, Glan–Thompson polarizer; S, sample; C, compensator; A, Glan–Thompson analyzer; PD, photodetector.

Table 3. Karl Lambrecht Wave Plates' Retardations at λ = 632.8 nm Measured Using Sénarmont Compensator Technique

Wave-Plate Type	Manufacturer's Retardation at λ = 632.8 nm	Measured Retardation
λ/2 mica 800 nm	404.70nm	409.39nm
λ/2 mica 780 nm	394.03nm	392.86nm

for larger retardations. Consequently, to produce a small retardation, two half-wave plates made of mica are used that are designed respectively for wavelengths equal to 780 nm and 800 nm. The wave plates were fabricated by Karl Lambrecht Corporation. Orientating both wave plates so their fast and slow axes are parallel allows a retardation equal to the difference between both wave plates' retardations to be produced. This principle is used to obtain a total retardation of ~10 nm. The second sample is the second type of Brace–Köhler compensator, model U-CBR2, and having a retardation equal to 21.54 nm at the wavelength of 546.1 nm. It is usually used to measure retardations less than λ/10.

Because the Karl Lambrecht wave plates are fabricated with an uncertainty of ±5 nm, they are first measured individually using the Sénarmont compensator technique and the configuration of Fig. 22. Table 3 shows a comparison of the measured retardations with the manufacturer's values. The manufacturer's values are calculated taking into account the birefringence dispersion of mica between the wavelengths for which the wave plates have been fabricated, i.e., 780 and 800 nm, and the wavelength 632.8 nm at which they are used. The retardations of both wave plates are measured at 632.8 nm and are found to be 392.86 nm and 409.39 nm, respectively. Combining both wave plates therefore allows a total retardation of 16.53 nm to be produced. This first sample is used to compare the Brace–Köhler, TWC, and Sénarmont techniques. A Karl Lambrecht wave plate is placed in a rotating dial in the light path and orientated at 45° from extinction. The second wave plate is placed in a rotating insert that is fixed at a position producing a minimum of intensity corresponding to the case where the fast and slow axes of both wave plates are parallel. The retardation is measured using the three techniques, and the error is calculated as a percentage of the exact retardation. This is summarized in Table 4. Of the three techniques, the TWC measured the retardation most accurately, producing an error of only 1.60%, whereas the Sénarmont and Brace–Köhler

Table 4. Comparison between the Brace–Köhler, TWC, and Sénarmont Compensator Techniques

Sample Retardation (nm)	Measurement Technique	Measured Retardation (nm)	Error (%)
16.53	Sénarmont	14.94	9.57
16.53	Brace–Köhler	15.56	5.80
16.53	TWC	16.26	1.60

Table 5. Further Comparison between the Brace–Köhler, TWC, and Sénarmont Compensator Techniques

Sample Retardation (nm)	Measurement Technique	Measured Retardation (nm)	Error (%)
21.78	Sénarmont	22.26	2.22
21.78	Brace–Köhler	21.62	0.74
21.78	TWC	21.81	0.13

techniques produced errors of 9.57% and 5.80%, respectively. The Brace–Köhler compensator model U-CBR2 is also used as a sample. Table 5 summarizes the results. The sample's retardation is recalculated for the wavelength of 632.8 nm, since the manufacturer's value is given for the wavelength of 546.1 nm. The TWC also measured this sample's retardation most accurately, producing an error of only 0.13%, whereas the Sénarmont and Brace–Köhler techniques produced errors of 2.2% and 0.74%, respectively.

5. Conclusions

The two wave-plate compensator technique is analyzed and developed for single-point retardation measurements. It consists of rotating a wave plate in a two-wave-plate system until a linearly polarized output is obtained that allows extinction to be produced by rotating the analyzer. The condition for linearly polarized output is derived as a function of the two wave plates' retardations without any approximations. Experimental procedures are developed to determine whether the sample or the compensator needs to be rotated to proceed to the measurement and to retrieve accurately the retardation. Unlike the Brace–Köhler method, the TWC technique is applicable for all retardations from 0 to λ. It is shown numerically that the TWC technique is more accurate than the Brace–Köhler method over a wider range of small retardations from 0 to $\lambda/8$. The TWC resolution is calculated to be 0.02 nm. Experimentally, the TWC method is compared with the Brace–Köhler and Sénarmont methods on samples with small retardations. For the two samples, the TWC produces relative errors of 1.60% and 0.13%, respectively, whereas the Brace–Köhler and Sénarmont techniques produce relative errors of 5.80% and 9.57% for the first sample and 0.74% and 2.2% for the second sample, respectively. The TWC technique proves to be more accurate than the Brace–Köhler and Sénarmont compensator techniques for single-point retardation measurements of small retardations. Future research involves the implementation of the TWC technique for full-field retardation measurements using a polarization microscope. This ultimately can be used for the accurate two-dimensional retrieval of natural or stress-induced birefringence in optical fibers and optical interconnects.

Appendix A: Intensity Along the Semiaxes of a Polarization Ellipse

By deriving the exact expression for the intensity along the semiaxes of the output polarization ellipse occurring for θ_2 equal to $\pm 45°$, general criteria for the resolution range of the TWC can be developed in terms of the input power I_o and the minimum intensity $I_{\min}$ measurable by the experimental system. Using Jones calculus, an electric field is represented with the phasor $\boldsymbol{\varepsilon}$, where

$$\boldsymbol{\varepsilon} = \begin{pmatrix} c_1 \exp(j\beta_1) \\ c_2 \exp(j\beta_2) \end{pmatrix}, \tag{39}$$

and where c_1 and c_2 are the amplitudes of the vibrations along the two polarization directions of the birefringent medium, and β_1 and β_2 are the phase shifts introduced to the two vibrations upon traveling through the birefringent medium. Assuming two vibrations, respectively $u(t)$ and $v(t)$ along the slow and fast axes of the birefringent medium, the ellipse traced by the electric field can be represented by $u(t) = c_1 \cos \omega t$ and $v(t) = c_2 \cos(\omega t + \beta_2 - \beta_1)$, with ωt the radian frequency. After transmission by the birefringent medium, it can be shown that the two semiaxes of the polarization ellipse traced by the electric field occur for the following radian frequencies ωt_1 and ωt_2,

$$\omega t_1 = -\frac{1}{2} \arctan \frac{{c_2}^2 \sin[2(\beta_2 - \beta_1)]}{{c_1}^2 + {c_2}^2 \cos[2(\beta_2 - \beta_1)]}, \tag{40}$$

$$\omega t_2 = \omega t_1 + 90°. \tag{41}$$

By substituting Eqs. (40) and (41) in Eqs. (25) through (28), the length of the semiaxes S_1 and S_2 of the polarization ellipse can be derived for $\theta_2 = \pm 45°$ as

$$S_1(\theta_2 = \pm 45°) = \cos\left(\frac{\phi_1 \pm \phi_2}{2}\right), \tag{42}$$

$$S_2(\theta_2 = \pm 45°) = \sin\left(\frac{\phi_1 \pm \phi_2}{2}\right). \tag{43}$$

To calculate the intensity along the semiaxes of the polarization ellipse, we use the fact that the intensity of the electric field is given by $\boldsymbol{\varepsilon} \cdot \boldsymbol{\varepsilon}^*$. Therefore the intensity I_s along the semiaxes of the polarization ellipse is

$$I_s(\theta_2 = \pm 45°) = S_i(\pm 45°)^2 I_o, \tag{44}$$

where i can have the value of 1 or 2, and I_o is the initial light source intensity.

This work was performed as part of the Interconnect Focus Center research program at the Georgia Institute of Technology and was supported by Microelectronics Advanced Research Corporation and Defense Advanced Research Projects Agency.

References

1. K. Kitamura, S. Kimura, Y. Miyazawa, Y. Mori, and O. Kamada, "Stress–birefringence associated with facets of rare-earth garnets grown from the melt; a model and measurement

of stress–birefringence observed in thin sections," J. Cryst. Growth **62,** 351–359 (1983).
2. K. Kitamura, Y. Miyazawa, Y. Mori, S. Kimura, and M. Higuchi, "Origin of difference in lattice spacings between on- and off-facet regions of rare-earth garnets grown from the melt," J. Cryst. Growth **64,** 207–216 (1983).
3. K. Kitamura, N. Lyi, and S. Kimura, "Growth-induced optical anisotropy of epitaxial garnet films grown on (110)-oriented substrates," J. Appl. Phys. **60,** 1486–1489 (1986).
4. K. Katoh, K. Hammar, P. Smith, and R. Oldenbourg, "Birefringence imaging directly reveals architectural dynamics of filamentous actin in living growth cones," Mol. Biol. Cell **10,** 197–210 (1999).
5. R. Oldenbourg, E. D. Salmon, and P. T. Tran, "Birefringence of single and bundled microtubules," Biophys. J. **74,** 645–654 (1998).
6. B. Cense and T. C. Chen, "*In vivo* depth-resolved birefringence measurements of the human retinal nerve fiber layer by polarization-sensitive optical coherence tomography," Opt. Lett. **27,** 1610–1612 (2002).
7. A. Redner, "Photoelastic measurements by means of computer-assisted spectral-contents analysis," Exp. Mech. **25,** 148–153 (1985).
8. A. Redner, "Photoelastic measurements of residual stresses for NDE," in *Photomechanics and Speckle Metrology*, F.-P. Chiang, ed., Proc. SPIE **814,** 16–19 (1987).
9. J. E. Houston, "The effect of stress on the nanomechanical properties of Au surfaces," in *Structure and Evolution of Surfaces*, R. Cammarata, ed., Proc. Mater. Res. Soc. **440,** 177–187 (1997).
10. E. D. Fabrizio, M. Baciocchi, M. Gentili, and L. Grella, "Microphotonic devices fabricated by silicon micromachining techniques," J. Appl. Phys. **36,** 7757–7762 (1997).
11. P. L. Chu and T. Whitbread, "Measurement of stresses in optical fiber and preform," Appl. Opt. **21,** 4241–4245 (1982).
12. X. Zhao, C. Li, and Y. Z. Xu, "Stress-induced birefringence control in optical planar waveguides," Opt. Lett. **28,** 564–566 (2003).
13. S. Y. Cheng, K. S. Chiang, and H. P. Chan, "Birefringence in benzocyclobutene strip optical waveguides," IEEE Photon. Technol. Lett. **15,** 700–702 (2003).
14. D. J. Wissuchek, C. W. Ponader, and J. J. Price, "Analysis of residual stress in optical fiber," in *Optical Fiber Reliability and Testing*, Proc. SPIE **3848,** 34–43 (1999).
15. G. W. Scherer, "Thermal stress in a cylinder: application to optical waveguide blanks," J. Non-Cryst. Solids **34,** 223–238 (1979).
16. C. S. Kim, Y. Han, B. H. Lee, W. T. Han, U. C. Paek, and Y. Chung, "Induction of the refractive index change in B-doped optical fibers through relaxation of the mechanical stress," Opt. Commun. **185,** 337–342 (2000).
17. D. A. Krohn, "Determination of axial stress in clad glass fibers," J. Am. Ceram. Soc. **53,** 505–507 (1970).
18. U. C. Paek and C. R. Kurkjian, "Calculation of cooling rate and induced stresses in drawing of optical fibers," J. Am. Ceram. Soc. **58,** 330–335 (1975).
19. B. H. Kim, Y. Park, D. Y. Kim, U. C. Paek, and W. T. Han, "Observation and analysis of residual stress development resulting from OH impurity in optical fibers," Opt. Lett. **27,** 806–808 (2002).
20. G. W. Scherer, "Stress-induced index profile distortion in optical waveguides," Appl. Opt. **19,** 2000–2006 (1980).
21. G. W. Scherer, "Stress-optical effects in optical waveguides," J. Non-Cryst. Solids **38,** 201–204 (1980).
22. K. Dossou, S. LaRochelle, and M. Fontaine, "Numerical analysis of the contribution of the transverse asymmetry in the photo-induced index change profile to the birefringence of optical fiber," J. Lightwave Technol. **20,** 1463–1469 (2002).
23. B. H. Kim, Y. Park, T. J. Ahan, D. Y. Kim, B. H. Lee, Y. Chung, U. C. Paek, and W. T. Han, "Residual stress relaxation in the core of optical fiber by CO_2 laser irradiation," Opt. Lett. **26,** 1657–1659 (2001).
24. B. H. Kim, T. J. Ahan, D. Y. Kim, B. H. Lee, Y. Chung, U. C. Paek, and W. T. Han, "Effect of CO_2 laser irradiation on the refractive-index change in optical fibers," Appl. Opt. **41,** 3809–3815 (2002).
25. Y. Park, T. J. Ahn, Y. H. Kim, W. T. Han, U. C. Paek, and D. Y. Kim, "Measurement method for profiling the residual stress and the strain–optic coefficient of an optical fiber," Appl. Opt. **41,** 21–26 (2001).
26. Y. Park, U. C. Paek, and D. Y. Kim, "Complete determination of the stress tensor of a polarization-maintaining fiber by photoelastic tomography," Opt. Lett. **27,** 1217–1219 (2002).
27. D. A. B. Miller, "Physical reasons for optical interconnection," Intl. J. Opt. **11,** 155–168 (1997).
28. L. G. Peralta, A. A. Bernussi, H. Temkin, M. M. Borhani, and D. E. Doucette, "Silicon-dioxide waveguides with low birefringence," IEEE J. Quantum Electron. **39,** 874–879 (2003).
29. A. Kilian, J. Kirchhof, B. Kuhlow, G. Przyrembel, and W. Wischmann, "Birefringence free planar optical waveguide made by flame hydrolysis deposition (FHD) through tailoring of the overcladding," J. Lightwave Technol. **18,** 193–198 (2000).
30. M. Huang, "Stress effects on the performance of optical waveguides," Intl. J. Solids Struct. **40,** 1615–1632 (2003).
31. A. Ajovalasit, S. Baronne, and G. Petrucci, "A review of automated methods for the collection and analysis of photoelastic data," J. Strain Anal. **33,** 75–91 (1998).
32. A. Ajovalasit, S. Baronne, and G. Petrucci, "Automated photoelasticity in white light: influences of quarter-wave plates," J. Strain Anal. **30,** 29–34 (1995).
33. T. C. Oakberg, "Measurement of low-level strain birefringence in optical elements using a photoelastic modulator," in *Polarization Analysis and Applications to Device*, T. Yoshizawa and H. Yokota, eds., Proc. SPIE **2873,** 17–20 (1996).
34. B. Wang and T. Oakberg, "A new instrument for measuring both magnitude and angle of low level linear birefringence," Rev. Sci. Instrum. **70,** 3847–3854 (1999).
35. M. M. Swann and J. M. Mitchison, "Refinements in polarized light microscopy," J. Exper. Biol. **27,** 226–237 (1950).
36. R. D. Allen and L. I. Rebhun, "Photoelectric measurement of small fluctuating retardations in weakly birefringent, light-scattering biological objects," Exp. Cell Res. **29,** 583–592 (1963).
37. R. Oldenbourg and G. Mei, "New polarized light microscope with precision universal compensator," J. Microsc. **180,** 140–147 (1995).
38. N. H. Hartshorne and A. Stuart, *Crystals And The Polarizing Microscope, A Handbook For Chemists And Others* (Edward Arnold, London, 1960).
39. G. S. Smith, *An Introduction to Classical Electromagnetic Radiation* (Cambridge University, New York, 1997).
40. B. Wang, "An improved method for measuring low-level linear birefringence in optical materials," in *Inorganic Optical Materials*, A. J. Marker III, ed., Proc. SPIE **3424,** 120–124 (1998).
41. B. Wang, "Accuracy assessment of a linear birefringence measurement system using a Soleil–Babinet compensator," Rev. Sci. Instrum. **72,** 4066–4070 (2001).
42. B. Wang, "Linear birefringence measurement instrument using two photoelastic modulators," Opt. Eng. **41,** 981–987 (2002).
43. C. C. Montarou and T. K. Gaylord, "Single-point two-waveplate compensator for optical retardation, thickness, and refractive index measurement," U.S. utility patent 60/506,381 (24 September 2004).